

# Surface waves and oceanic mixing: Insights from numerical simulations with stochastic surface forcing

P. P. Sullivan

National Center for Atmospheric Research, Boulder, CO, USA

J. C. McWilliams

Department of Atmospheric and Oceanic Sciences and Institute of Geophysics and Planetary Physics, UCLA, Los Angeles, CA, USA

W. K. Melville

Scripps Institution of Oceanography, University of California, San Diego, La Jolla, CA, USA

**Abstract.** A large-eddy simulation (LES) model for oceanic boundary layers (OBLs) is developed that includes influences of surface waves for the special situation of wind-wave equilibrium. The wave processes included are conservative wave-current interactions (vortex force and material advection by Stokes drift), derived from an asymptotic theory, and non-conservative impacts of wave breaking, modeled as compact stochastic impulses. These influences are evaluated separately and in combination, and are compared to results from uniform (constant) stress-driven boundary layers. Results show that surface waves can enhance oceanic mixing over a significant fraction of the mixed-layer depth and the combined action of Stokes drift and intermittent wave breaking generates the greatest mixing. Their combined effect is to generate a newly identified coherent structure (in addition to the familiar Langmuir circulation due to the vortex force), a downwelling jet that efficiently transports momentum and scalars over the depth of the OBL. A crucial input to these simulations is the probability density function of breaker phase speeds,  $p[c]$ , and hence there is a critical need to better understand and parameterize the distribution of breaking waves at the sea surface under high wind conditions.

## Introduction

In high-wind conditions the sea surface is a mosaic of interacting dynamic and thermodynamic processes. Spray, bubbles, sea-surface heterogeneities, and waves are just a few of the interfacial processes coupling the atmospheric and oceanic boundary layers over a broad spectrum of temporal and spatial scales. The development and evolution of tropical cyclones [Emanuel, 2004] is a vivid example of the couplings between small-scale processes in the planetary boundary layers and large-scale dynamics. On the water side of the air-sea interface oceanic mixing is powered by complex surface dynamics (see Figure 1) featuring turbulent wind gusts, highly intermittent breaking waves, and wave-current interactions due to the Lagrangian mean wave current, Stokes

drift (i.e., Langmuir circulations). For winds exceeding moderate strength ( $6\text{--}8\text{ m s}^{-1}$ ), momentum and energy is thought to be transferred to the water primarily through the wave field [Donelan, 1998, 2001], and wave transfer effects may well be significant at lower winds, though harder to detect. Hence wave dynamics, not viscous and diffusive processes, can determine the surface boundary fluxes of momentum, energy, and scalars, and ultimately the vertical mixing of the oceanic boundary layer (OBL). The considerable complexity exhibited in Figure 1 is replaced, by convention and presumed necessity, in most 1-D oceanic boundary-layer models by a mean stress-driven layer that ignores wave-current interactions and collapses intermittent turbulence and wave breaking processes into ensemble averages

[Craig, 1996; Craig and Banner, 1994; Kantha and Clayson, 2004]. The present modeling investigation attempts to go beyond the ensemble view by examining the impact of two particular wave processes, viz., wave-current interactions from Stokes drift and transient wave breaking, on oceanic mixing using turbulence resolving large-eddy simulation (LES) of the OBL. However, given the flow complexity this can only be done in highly idealized ways.

The LES model we use is a conventional one [Moeng, 1984] except for the representation of surface-wave effects: it is based on the incompressible Navier-Stokes Equations under a Boussinesq approximation with a flat top surface (mean sea level) and a subgrid-scale parameterization by single-point, second-moment turbulent kinetic energy (TKE) closure. The added wave effects are the vortex force and Lagrangian mean advection associated with Stokes drift,  $\mathbf{u}^{St}$ , and a wave-averaged increment to the pressure that arise through conservative wave-current interaction [McWilliams *et al.*, 1997], as well as additional acceleration and energy generation due to non-conservative wave breaking [Sullivan *et al.*, 2004]. The governing equations for momentum, subgrid-scale TKE, and density incorporating the above wave influences are not repeated here but can be found in Sullivan *et al.* [2005].

## Wind-wave equilibrium

For modeling wave effects in the surface boundary layer, we must specify both the wave spectrum to determine Stokes drift profile and the distribution (spectrum) of breaking waves for transfer of momentum and kinetic energy to the underlying water. In both cases our primary interest is the situation of wind-wave equilibrium where the wave spectrum is fully developed and the atmospheric inputs of momentum and energy flux are perhaps best characterized by observations. Full development refers to an asymptotic state in which the energy density, the peak frequency, and the shape of the wave spectrum are not changing with time. Then the frequency spectrum of wave heights  $F(f)$  is well described by the empirical expression [Donelan *et al.*, 1985; Alves *et al.*, 2003]

$$F\left(\frac{\sigma}{2\pi} = f\right) = \alpha_w \frac{g^2}{f_p^4} \exp \left[ - \left( \frac{f}{f_p} \right)^{-4} \right] \quad (1)$$

where  $\alpha_w$  is the ‘‘Phillips constant’’,  $g$  is the gravitational acceleration, and  $f_p$  is the peak in the spectrum related to a reference atmospheric wind  $U_a(z = 10 \text{ m})$  by

$$f_p = \nu \frac{g}{U_a}, \quad \nu \approx 0.123. \quad (2)$$

The atmospheric inputs to the ocean are most often expressed as bulk aerodynamic formulas for the density-normal-

ized stress  $\boldsymbol{\tau}$  and energy  $\mathcal{E}$  fluxes in the forms [Liu *et al.*, 1979; Terray *et al.*, 1996]

$$\boldsymbol{\tau} = \frac{\rho_a}{\rho_o} C_D U_a^2 \quad \text{and} \quad \mathcal{E} = m \left( \frac{\rho_o}{\rho_a} \right)^{1/2} \tau^{3/2}, \quad (3)$$

where  $\rho_{a,o}$  are reference densities of the atmosphere and ocean, the drag coefficient  $C_D \approx 10^{-3}$  is a function of  $U_a$ , and the energy flux constant  $m \approx 3.5$  (see figure 8 of Terray *et al.* [1996]). The water friction velocity  $u_* = \sqrt{\tau}$ .

## Wave-current interactions

Wave-averaged dynamical effects on currents are the result of an asymptotic theory first derived by Craik and Leibovich [1976] and then extended by McWilliams and Restrepo [1999]; McWilliams *et al.* [2004]. These effects enter into our LES model as Stokes advection in the TKE and scalar equations and as a generalized vortex force,

$$\frac{\partial \bar{\mathbf{u}}}{\partial t} = \dots + \mathbf{u}^{St} \times (f \hat{\mathbf{z}} + \bar{\boldsymbol{\omega}}), \quad (4)$$

in the resolved scale momentum equation ( $f$  is the Coriolis parameter and the resolved vorticity  $\bar{\boldsymbol{\omega}} = \nabla \times \bar{\mathbf{u}}$ ). The vortex force has a significant influence on the turbulent eddies and their vertical fluxes in the OBL through the generation of Langmuir circulations [Craik and Leibovich, 1976; McWilliams *et al.*, 1997]. Wave effects also appear in the subgrid-scale energy ( $e$ ) equation primarily as a Stokes production term,

$$\frac{\partial e}{\partial t} = \dots - \tau_{ij} \frac{\partial u_i^{St}}{\partial x_j}, \quad (5)$$

i.e., subgrid-scale stresses  $\tau_{ij}$  working on the vertical gradient of the Stokes drift. An analogous term appears in the TKE balance for resolved scales [McWilliams *et al.* [1997, equation 5.1]], and we note Stokes production has recently been included in some one-dimensional, Reynolds-averaged models of the OBL, [Kantha and Clayson, 2004]. There is an additional conservative wave-averaged effect in the resolved material scalar concentration ( $\bar{c}$ ) equation,

$$\frac{\partial \bar{c}}{\partial t} = \dots - \mathbf{u}^{St} \cdot \nabla \bar{c}. \quad (6)$$

The vertical profile of Stokes drift is thus a primary input to LES with wave-averaged effects. Past LES typically estimate  $u^{St}(z)$  from a single monochromatic wave [McWilliams *et al.*, 1997; Skillingstad and Denbo, 1995] chosen to approximate a dominant component in the wave spectrum. In our wind-wave equilibrium situation, we use (1) and employ numerical quadrature to evaluate

$$u^{St}(z) = \frac{2}{g} \int_0^\infty F(\sigma) \sigma^3 \exp \left[ \frac{2\sigma^2 z}{g} \right] d\sigma \quad (7)$$

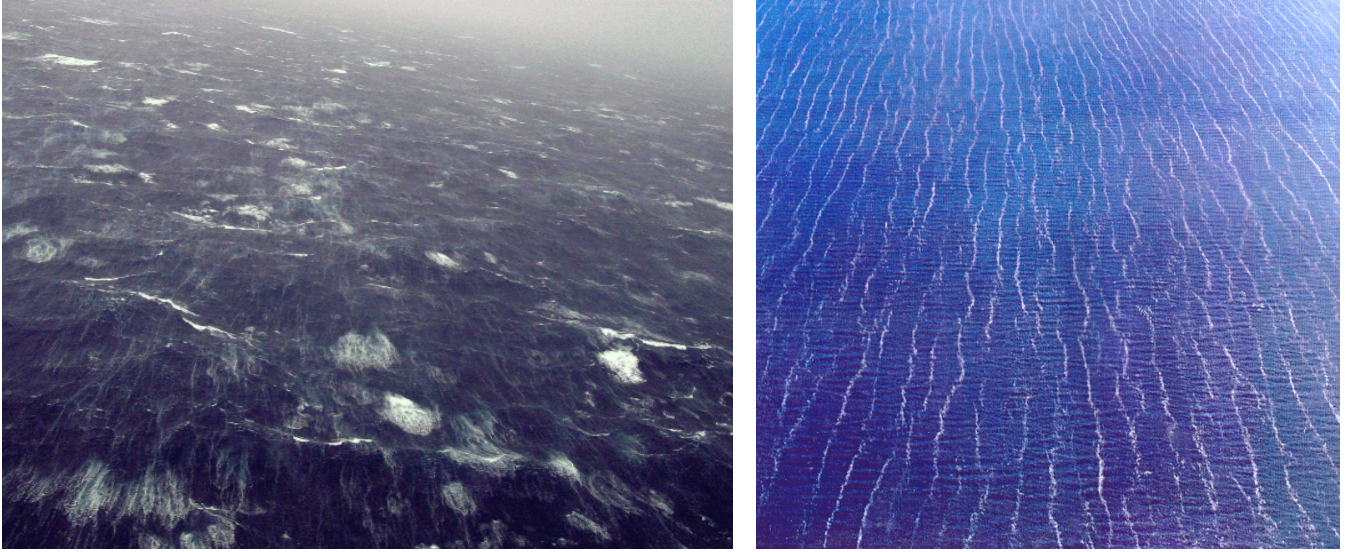


**Figure 1.** (left panel) Sea surface beneath hurricane Isabel dominated by breaking waves of multiple scales (courtesy P. Black) and (right panel) foam lines tracking the formation of Langmuir circulations in the Great Salt Lake (courtesy S. Monismith).

following the procedure described by *McWilliams and Restrepo* [1999] and *Kenyon* [1969]. Compared to past LES implementations, the vertical profile of  $u^{St}(z)$  from (7) exhibits a sharper near-surface gradient due to the inclusion of high-wavenumber components in the wave spectrum.

### Stochastic breakers

The second wave process we wish to incorporate in our modeling, transient breaking waves, is motivated by the visual impression of the sea surface in Figure 1. We view the waves as an intermediate reservoir that releases momentum to the underlying water in localized intermittent impulses, and the primary path from wind drag to current generation is through wave breaking. The momentum passed to the OBL is then a summation of randomly occurring events in space and time. *Donelan* [1998, 2001] support this view and show that almost 100% of the momentum stored in the wave field leaves locally, entering the water through wave breaking. Here, we only attempt to capture the bulk features of these intermittent events since our target is the effects of breakers on larger scale OBL turbulence.

Global conservation laws provide bounds on the average amount of momentum and energy exchanged between the atmosphere and ocean but clearly do not constrain the local space-time flux transfer from an individual breaking event. In the open ocean wave breaking is sufficiently complicated and poorly understood that we are forced to rely on a large input of empirical information for our discrete event modeling. We begin by noting in wind-wave equilibrium the av-

erage momentum flux into the wave field from the wind is balanced by the net momentum flux from waves to currents. Thus, the long-time, large-area total momentum conservation rule expressed in terms of the horizontal momentum flux,  $\tau$ , from the atmosphere over an area of surface water,  $A_L$ , and time period,  $T_L$ , is

$$\tau = \tau_v + \frac{\overline{M}_b}{\rho_o A_L T_L}, \quad (8)$$

where  $\overline{M}_b$  is the total momentum contained in a field of resolved-scale breakers and  $\tau_v$  is an unresolved (or background) stress acting at the water surface.  $\tau_v$  accounts for viscous stresses at low wind speeds or small scale breakers that fall below the mesh resolution of the LES. In (8) the momentum supplied to the currents is the integrated effect of randomly occurring events of varying size, speed, and orientation

$$\overline{M}_b = N \int^\Theta \int^c p[c, \Theta] \overline{M}(c, \Theta) dc d\Theta. \quad (9)$$

$p[c, \Theta]$  is the probability density function (PDF) of breaker speeds  $c$  with orientation  $\Theta$ ,  $N$  is the total number of breakers in the time period  $T_L$  over surface area  $A_L$ , and  $\overline{M}(c, \Theta)$  is the momentum imparted by an individual breaker. In *Sullivan et al.* [2004] we proposed a discrete model for  $\overline{M}(c)$  that is fully three dimensional and time varying. The basis of the model is the assumption of Froude scaling, using the linear dispersion relationship to relate the length and time scales of the breaking event, consistent with the labora-

tory measurements of *Melville et al.* [2002] and earlier measurements cited therein. Then a single wave property, *viz.*, the phase speed  $c$ , is sufficient to define the breaker wavelength  $\lambda$ , period  $T$ , and wavenumber  $k$ . Our model is assumed to be rectilinear, as a breaker evolves over its lifetime  $t_o < t < t_o + T(c)$  it expands horizontally in  $x$  and deepens in  $z$  with its spanwise extent  $\lambda$  held fixed.

Given a wind speed  $U_a$ , breaker impulse  $\overline{\mathcal{M}}$ , and distribution  $p[c, \Theta]$ , substitution of (9) into (8) defines the *average* rate of breaker creation

$$\dot{N} = \frac{N}{A_L T_L}, \quad (10)$$

in units of  $\text{m}^{-2}\text{s}^{-1}$ .  $\dot{N}$  directly impacts the LES. For a specific problem setup, as the solutions are stepped forward in time, random draws from the PDF are made at a rate  $\dot{N}$  so that the long-time, large-area average momentum in the water matches the atmospheric input.

## The PDF of breaking waves

The final piece in our modeling is the specification of the PDF of breaking for typical open-ocean conditions. The initial simplification we impose is to ignore any angular dependence so that  $p[c, \Theta] \rightarrow p[c]$  (also  $\overline{\mathcal{M}}(c, \Theta) \rightarrow \overline{\mathcal{M}}(c)$ ). We appeal to the field measurements of *Melville and Matusov* [2002], who used a novel airborne video system to measure the kinematics of breaking over a limited set of wind speeds and fetch. They digitized video images to obtain estimates of  $\Lambda(c)$  the average length of breaking crests per unit area traveling at velocities in the range  $(c, c + dc)$ . Combining  $\Lambda(c)$  with our rectilinear breaking model implies

$$p[c] = k_p \frac{\Lambda(c)}{\lambda(c)} = \frac{k_p g}{2\pi} \frac{\Lambda(c)}{c^2} \quad (11)$$

using the linear dispersion relation. The constant  $k_p$  scales the PDF so that  $\int_0^\infty p[c] dc = 1$ . A curve fit of the observations gives (see Figure 2)

$$p[c] = \frac{k_p g}{2\pi} \frac{U_a^3 \exp(-0.64c)}{c^2}. \quad (12)$$

We note that the observations are only able to detect visible whitecaps (i.e., those where air is actively entrained during the breaking process), and were truncated at  $c \approx 1 \text{ m/s}$ . Hence small scale breakers and breakers without significant air entrainment will not be accounted for by these measurements nor by the PDF. *Melville and Matusov* [2002] find that the magnitude of  $\Lambda(c)$  scales as  $U_a^3$  in agreement with *Phillips* [1985, p. 528]. However, the dynamic range of the measurements is not sufficient to capture the variation

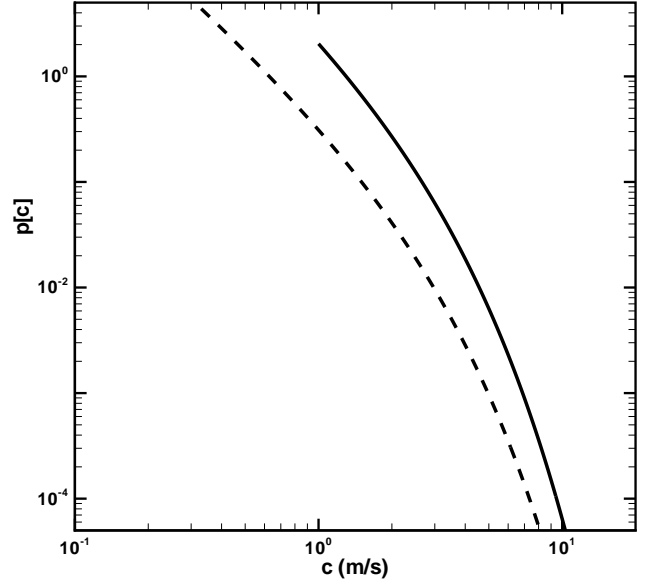


**Figure 2.** The probability density function of breaking phase speeds  $p[c]$ . The solid line is the PDF given by (12) that is based on the measurements of *Melville and Matusov* [2002] at  $U_a = 10 \text{ m s}^{-1}$ . The dashed line is the PDF of the same functional form but now with hard cutoff limits at the lower and upper endpoints according to *Phillips* [1985].

at small and large  $c$ . The behavior of  $\Lambda(c)$  at its endpoints is important as this introduces an additional wind speed dependence into the measured PDF. See *Phillips* [1985] and the Discussion below.

## Illustrative results

The various pieces of our wave modeling ideas are currently being implemented and evaluated in an LES model for the OBL over a range of wind speeds. This has proven to be an iterative task, and at the present time is not yet complete. Here we show preliminary results using the PDF based on the measurements of  $\Lambda(c)$  shown in Figure 2. We expect the following results to be qualitatively representative of future more complete LES solutions that take into account the wind speed dependence of the breaker spectrum endpoints.

The suite of LES experiments compares OBL solutions of four types: the conventional posing with uniform stress, without any wave effects; the conventional posing plus wave-averaged Stokes drift terms [*McWilliams et al.*, 1997]; a posing with stochastic forcing representing breaking waves; and, a posing with stochastic forcing plus Stokes drift terms (see Table 1 for naming and labeling conventions used in the figures). For this investigation we choose a reference wind

**Table 1.** Simulation properties

Name	Forcing	Stokes drift	Symbol line
U	uniform stress	No	black/dash-dot
U+ST	uniform stress	Yes	red solid
B	100% breaking	No	blue solid
B+ST	100% breaking	Yes	black solid

$U_a = 10 \text{ m s}^{-1}$  and a small surface heat flux  $Q_* = 2 \text{ W m}^{-2}$ . This fixes the atmospheric momentum and energy fluxes and the equilibrium wave field. For this wind speed, the atmospheric drag coefficient  $C_d = 0.0013$  based on the model of *Liu et al.* [1979], water friction velocity  $u_* = 0.011 \text{ m s}^{-1}$ , the Stokes drift  $u^{St}(z = -1 \text{ m}) = 0.1 \text{ m s}^{-1}$ , and the turbulent Langmuir number  $La_t = \sqrt{(u_*/u^{St})} \approx 0.3$ . Initially, the mixed layer is neutrally stratified over the depth  $h = -32 \text{ m} < z < 0$ . Below  $h$ , the water is stably stratified with the temperature decreasing at a constant rate of  $0.05 \text{ K m}^{-1}$ .

The basic numerical algorithm is fully described in *Sullivan et al.* [1994, 1996]; *McWilliams et al.* [1997]; *Sullivan et al.* [2004]. Numerical testing shows that the stochastic breaker forcing requires special treatment in the LES code in order to capture its full impact over the wide range of breaker scales. We employ a novel strategy that integrates the breaker forcing on a separate fine spatial mesh and subsequently averages the breaker forcing to the LES grid. This scheme conserves the total momentum from a breaker irrespective of its time and space scale and hence even small scale breakers are “felt” in the LES grid. Random draws are made from the PDF of breaker speeds at a rate so that the momentum imparted to the water matches the input supplied by the atmosphere. The initial location of a breaker at the water surface is drawn from a uniform PDF (see discussion in *Sullivan et al.* [2004]).

The computational domain  $(L_x, L_y, L_z) = (300, 300, -110) \text{ m}$  is discretized with  $(300, 300, 128)$  gridpoints, thus the constant horizontal grid spacing  $(\Delta x, \Delta y) = 1.0 \text{ m}$ . Vertical meshes are generated using constant algebraic stretching with the ratio of any two vertical cells  $K = \Delta z_{k+1}/\Delta z_k = 1.012$  held constant. All simulations are run for approximately 10 (physical) hours which takes about 50,000 computational steps. As is customary practice, statistics are generated by combining spatial  $x - y$  and temporal averaging.

The observed response of the OBL to vortex forces and wave breaking suggests a close connection between the surface wave conditions and vertical mixing in the OBL. We find that the mean currents, turbulence variances (and TKE),

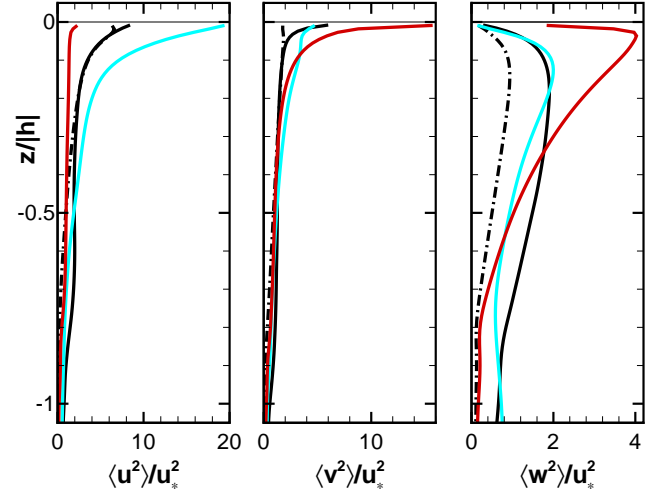


**Figure 3.** Mean square variances for cases with no wave effects (dash-dot line), Stokes drift (red line), wave breaking (blue line), and Stokes drift plus breaking (black line).

scalar and momentum fluxes, and entrainment at the thermocline all exhibit a sensitivity to the surface wave field. One of the most striking results is the greatest mixing arises when wave breaking and Langmuir circulations (resulting from Stokes drift) act together. In general simulations with explicit wave influences differ from their counterparts driven by constant stress and no wave effects. Some of the statistical evidence from the LES is displayed in Figures 3, 4, and 5. Inspection of the turbulence variance profiles (see Figure 3) highlights the competition and trade-offs between breaking and Stokes drift compared to the flow with the same average forcing but with no wave effects. In simulation B, individual breakers impart a forward impulse and generate a near surface vortex [*Sullivan et al.*, 2004]. The cumulative effect of all breakers is to enhance the  $(u, w)$ -variances in the region  $-0.3 < z/h < 0$  compared to the case with no wave effects (simulation U). In the simulation with constant stress and Stokes drift streamwise oriented Langmuir vortices form [*McWilliams et al.*, 1997] that amplify the  $(v, w)$ -variances at the expense of the  $u$ -variance. In simulation B+ST, the two wave effects both compete and organize; breakers tend to lessen the spanwise coherence of the Langmuir vortices, but they also act together to noticeably amplify the vertical velocity. Near the water surface the magnitude of the  $w$ -variance increases by a factor of almost two for case B+ST compared to cases B and U+ST. This increase in  $w$ -variance enhances the vertical mixing in the OBL over a significant depth.

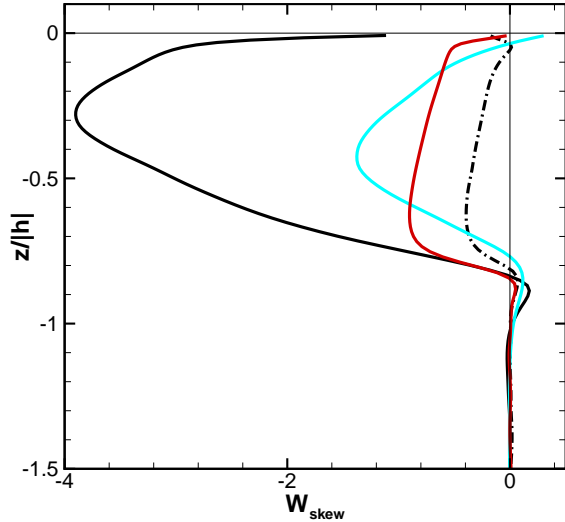


**Figure 4.** Vertical profiles of vertical velocity skewness for cases with no wave effects (dash-dot line), Stokes drift (red line), wave breaking (blue line), and Stokes drift plus breaking (black line).

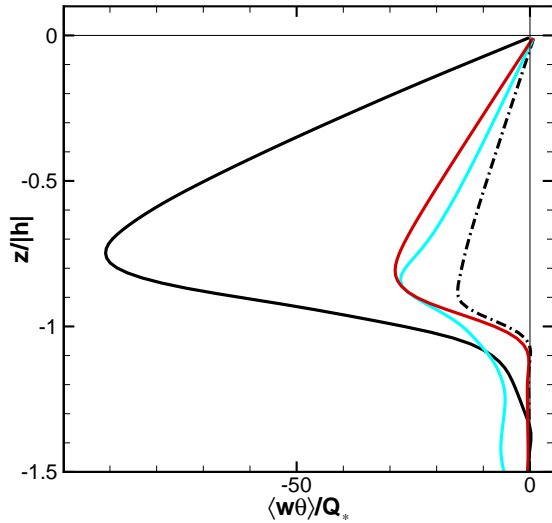


**Figure 5.** Vertical scalar flux normalized by its surface value. Simulations are cases with no wave effects (dash-dot line), Stokes drift (red line), wave breaking (blue line), and Stokes drift plus breaking (black line).

The vertical velocity skewness  $\langle w^3 \rangle / \langle w^2 \rangle^{3/2}$ , shown in Figure 4, further illustrates the synergistic behavior that can occur when breaking and Langmuir cells act together. *Moeng and Rotunno* [1990] find that a bias in vertical velocity skewness is one of the statistical measures indicating the presence of coherent structures in convective flows. Thus, the large negative skewness observed in the present flow with breaking and Stokes drift suggests that the two wave effects have potentially combined to form a coherent structure roughly analogous to a thermal plume. In order to examine this possibility, we performed extensive visualization of the LES solutions and present typical snapshots of  $w$  in  $x - y$  planes at selected vertical locations in Figure 6. These pictures along with animations of other LES solution variables do indeed reveal the existence and life cycles of vigorous “downwelling jets”.

We find that the origin of the downwelling jets can be traced to sites where breaking first occurs. At the water surface, the forward and local impulse from an intermittent breaker supplies an excess of horizontal momentum compared to the average background state. Previous studies have found that breaker debris can persist for multiple wave periods [Melville *et al.*, 2002; Sullivan *et al.*, 2004] despite the limited lifespan of active breaking, a time scale of order  $\lambda/c = 2\pi c/g$ . Thus remnants from the breaking process are available to fully interact with the Stokes drift. Our visualization shows leftover breaker momentum being advected forward and then squeezed laterally by the relentless action of Langmuir vortices. Particle tracing in our previous LES [McWilliams *et al.*, 1997] indicate how this convergence process leads to a dense concentration of particles and the subsequent merging of individual particle lines. The convergence of foam into forward looking Y-junctions is clearly visible in Figure 1. These same mechanisms are at work here, but now act on the momentum supplied by breaking. At a convergence point (or Y-junction) the excess horizontal motions are deflected sharply downward and emerge beneath the water surface in the form of vigorous downwelling jets. In a neutrally stratified OBL these structures penetrate to considerable depths and play important roles in setting the structure and mixing of the OBL. We find that the scale and intensity of the downwelling jets varies as expected with the breaker phase speed  $c$ .

The downwelling jets in Figure 6 play a critical role in setting the scalar mixing efficiency of the OBL (see Figure 5). The entrainment of cooler water from below the thermocline increases by almost a factor of six in the simulations with both wave breaking and Stokes drift. At the same time, these coherent structures alter the shape of the thermocline temperature profile and potentially are powerful enough to excite internal gravity waves.

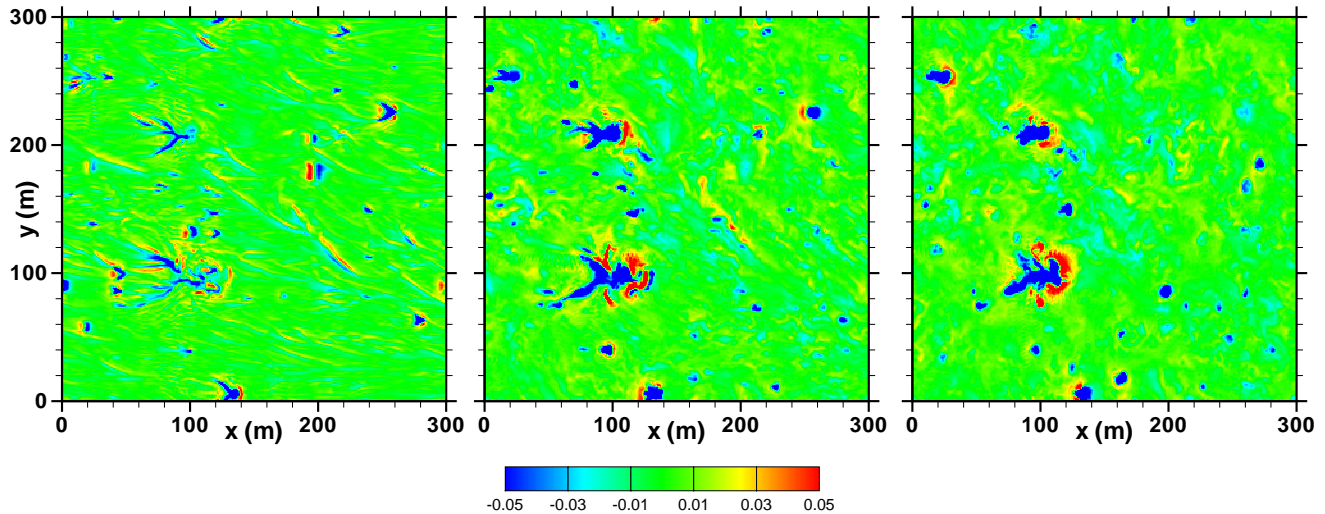


**Figure 6.** Snapshots of vertical velocity in  $x - y$  planes from an LES with intermittent breaking waves plus Stokes drift. Panels (left, middle, right) correspond to  $z = -(1.5, 6.1, 11)$  m. The color bar is in units of  $\text{m s}^{-1}$ . Notice close to the surface (left panel) how the combination of Langmuir cells and breaking waves generate strong downwelling (blue shading) in the form of a Y-junction. Deeper in the water (middle and right panels), the surface organization appears in the form of a roughly circular downwelling jet. The upwelling motions (red shading) are induced by a ring vortex that develops as the jet descends.

## Discussion

These first simulations hint that the impact of wave breaking at high winds is not confined to the oceanic surface layer but can act in concert with Langmuir circulations to greatly enhance OBL mixing and entrainment. (Langmuir circulations themselves penetrate throughout the boundary layer in these simulations even in the absence of breaking [McWilliams *et al.*, 1997].) A preliminary sweep across the wind regime,  $7.5 \text{ m s}^{-1} < U_a < 15 \text{ m s}^{-1}$  shows that these downwelling jets are robust, play active roles in the mixed layer, and enhance entrainment at the thermocline. These results contrast with those of Noh *et al.* [2004] who found no such structures when wave breaking is modeled by stochastic uniform noise at the water surface.

While we expect the qualitative features of these simulations to be robust, the details will depend on the specific inputs to the model. Perhaps the most significant of these is the PDF of the breakers as a function of  $U_a$  (or  $u_*$ ) and  $c$ . In this work we have used the measurements of  $\Lambda(c)$  by Melville and Matusov [2002] to infer the PDF for an equilibrium wave field at a wind speed of  $U_a = 10 \text{ m s}^{-1}$ . The PDF,  $p[c]$ , was bounded below by the  $1 \text{ m s}^{-1}$  cutoff in the measurements, and above by  $U_a$ . However, in the observations, the low-speed limit was determined by the visible limit of the whitecaps rather than the dynamical limit that one might obtain for breaking waves with no visible air en-

trainment. If, following Phillips [1985] we take the lower limit to be  $c \approx u_*$ , then the PDF will change significantly; leading to a shift in the peak of the PDF to lower values of  $c$  and a reduction of the PDF at larger  $c$ , as shown in Figure 2. This would lead to more frequent breaking at smaller scales (smaller  $c$ ) and less frequent breaking at larger scales. The empirical  $U_a^3$  dependence leads to a shift of breaking to larger scales as  $U_a$  increases. However, with the rapid decrease of  $\Lambda(c)$  as  $c$  increases, the measurements of Melville and Matusov [2002] do not show a clear cutoff at large  $c$ , which is expected to occur for  $c \approx U_a$ . We believe that the measurements are merging into the noise at large  $c$ .

In view of the limited measurements of breaking statistics, we also plan to conduct model runs using  $p[c]$  based on the theory of equilibrium wind waves first proposed by Phillips [1985]. In this theory, the equilibrium range is loosely defined as  $k_p < k < k_1$ , where  $k_p$  is the wavenumber of the peak in the wave spectrum and  $k_1$  is a high-wavenumber cut-off to the range, where  $k_p$  and  $k_1$  both vary with wind speed:  $\sim g/U_a^2$  and  $\sim g/u_*^2$ , respectively. In this range, the wave-dissipation spectrum varies as  $1/k$ . Integration of the wave-dissipation and momentum-flux spectra over all wavenumbers and matching the resulting expressions to the bulk formula in (3) leads to a strongly wind-speed dependent PDF. The strong variation of  $p[c]$  with  $U_a$  is due to both the strong dependence of  $\Lambda(c)$  on  $c$ , and the wind-speed variation of the cutoff wavenumbers, i.e.,

$(k_p, k_1) = f(U_a)$ , which significantly focuses breaking toward larger scales as  $U_a$  increases. However, discrepancies between the observed surface wavenumber spectra and those predicted by Phillips [1985] suggest that Phillip's equilibrium range may not extend out to  $k_1$  as defined above. Thus we expect that the development of consistent breaking models, with refined estimates of  $p[c]$ , will also lead to improved insight into wave spectral models.

The above predictions need to be validated against observations in high-wind conditions. A central quantitative issue is the breaker spectrum as a function of wind speed, which is needed as empirical input in the modeling approach we have taken here. For example, the wind speed  $U_a$  above which the equilibrium momentum flux  $\tau$  occurs primarily on the resolved scale, hence is appropriately modeled as stochastic impulses, needs to be determined. In this regime downwelling jets can be prominent features in the LES solution. Nevertheless, we feel confident that this phenomenon is likely to be important in a sufficiently high-wind regime. Given its strong enhancement of the boundary-layer entrainment rate, it might, e.g., play an important role in cooling the surface temperature and limiting the air-sea enthalpy supply under hurricanes. We look forward to exploring these issues further.

**Acknowledgments.** NCAR is sponsored by the National Science Foundation. PPS and WKM are supported by ONR (CBLAST) and NSF (Physical Oceanography).

## References

- Alves, J. G. M., M. L. Banner, and I. R. Young, Revisiting the Pierson-Moskowitz asymptotic limits for fully developed wind waves, *J. Phys. Oceanogr.*, **33**, 1301–1323, 2003.
- Craig, P. D., Velocity profiles and surface roughness under breaking waves, *J. Geophys. Res.*, **101**, 1265–1277, 1996.
- Craig, P. D., and M. L. Banner, Modeling wave-enhanced turbulence in the ocean surface layer, *J. Phys. Oceanogr.*, **24**, 2546–2559, 1994.
- Craik, A., and S. Leibovich, A rational model for Langmuir circulations, *J. Fluid Mech.*, **73**, 401–426, 1976.
- Donelan, M. A., Air-water exchange processes, in *Physical Processes in Lakes and Oceans*, vol. 54 of *Coastal and Estuarine Studies*, pp. 19–36, American Geophysical Union, 1998.
- Donelan, M. A., A nonlinear dissipation function due to wave breaking, in *Workshop on Ocean Wave Forecasting*, European Center for Medium Range Weather Forecasting, Reading, England, 2001.
- Donelan, M. A., J. Hamilton, and W. H. Hui, Directional spectra of wind-generated waves, *Phil. Trans. Roy. Soc. London, Ser. A*, **315**, 509–562, 1985.
- Emanuel, K., Tropical cyclone energetics and structure, in *Atmospheric Turbulence and Mesoscale Meteorology*, edited by E. Fedorovich, R. Rotunno, and B. Stevens, pp. 165–191, Cambridge University Press, 2004.
- Kantha, L. H., and C. A. Clayson, On the effect of surface gravity waves on mixing in the oceanic mixed layer, *Ocean Modelling*, **6**, 101–124, 2004.
- Kenyon, K. E., Stokes drift for random gravity waves, *J. Geophys. Res.*, **74**, 6991–6994, 1969.
- Liu, W. T., K. B. Katsaros, and J. A. Businger, Bulk parameterization of air-sea exchanges in heat and water vapor including the molecular constraints at the interface, *J. Atmos. Sci.*, **36**, 1722–1735, 1979.
- McWilliams, J. C., and J. M. Restrepo, The wave-driven ocean circulation, *J. Phys. Oceanogr.*, **29**, 2523–2540, 1999.
- McWilliams, J. C., P. P. Sullivan, and C.-H. Moeng, Langmuir turbulence in the ocean, *J. Fluid Mech.*, **334**, 1–30, 1997.
- McWilliams, J. C., J. R. Restrepo, and E. Lane, An asymptotic theory for the interaction of waves and currents in shallow coastal water, *J. Fluid Mech.*, **511**, 135–178, 2004.
- Melville, W. K., and P. Matusov, Distribution of breaking waves at the ocean surface, *Nature*, **417**, 58–63, 2002.
- Melville, W. K., F. Veron, and C. J. White, The velocity field under breaking waves: Coherent structures and turbulence, *J. Fluid Mech.*, **454**, 203–233, 2002.
- Moeng, C.-H., A large-eddy simulation model for the study of planetary boundary-layer turbulence, *J. Atmos. Sci.*, **41**, 2052–2062, 1984.
- Moeng, C.-H., and R. Rotunno, Vertical velocity skewness in the buoyancy-driven boundary layer, *J. Atmos. Sci.*, **47**, 1149–1162, 1990.
- Noh, Y., H. S. Min, and S. Raasch, Large eddy simulation of the ocean mixed layer: The effects of wave breaking and Langmuir circulation, *J. Phys. Oceanogr.*, **34**, 720–735, 2004.
- Phillips, O. M., Spectral and statistical properties of the equilibrium range in wind-generated gravity waves, *J. Fluid Mech.*, **156**, 505–531, 1985.
- Skyllingstad, E. D., and D. W. Denbo, An ocean large-eddy simulation of Langmuir circulations and convection in the surface mixed layer, *J. Geophys. Res.*, **100**, 8501–8522, 1995.
- Sullivan, P. P., J. C. McWilliams, and C.-H. Moeng, A subgrid-scale model for large-eddy simulation of planetary boundary-layer flows, *Boundary-Layer Meteorol.*, **71**, 247–276, 1994.
- Sullivan, P. P., J. C. McWilliams, and C.-H. Moeng, A grid nesting method for large-eddy simulation of planetary boundary layer flows, *Boundary-Layer Meteorol.*, **80**, 167–202, 1996.
- Sullivan, P. P., J. C. McWilliams, and W. K. Melville, The oceanic boundary layer driven by wave breaking with stochastic variability. I: Direct numerical simulations, *J. Fluid Mech.*, **507**, 143–174, 2004.
- Sullivan, P. P., J. C. McWilliams, and W. K. Melville, Surface gravity wave effects in the oceanic boundary layer: LES with vortex forces and stochastic breakers, *in preparation*, 2005.
- Terray, E. A., M. A. Donelan, Y. C. Agrawal, W. M. Drennan, A. J. W. K. K. Kahma, P. A. Hwang, and S. A. Kitaigorodskii, Estimates of kinetic energy dissipation under breaking waves, *J. Phys. Oceanogr.*, **26**, 792–807, 1996.